HHS Public Access

Author manuscript

J Am Chem Soc. Author manuscript; available in PMC 2019 April 04.

Published in final edited form as:

J Am Chem Soc. 2018 April 04; 140(13): 4485–4488. doi:10.1021/jacs.8b00887.

Photochemical Barcodes

Sicheng Tang[†], **Yang Zhang**[†], **Pravat Dhakal**[†], **Laura Ravelo**, **Cheyenne L. Anderson**, **Kevin M. Collins**, and **Françisco M. Raymo**[*]

Laboratory for Molecular Photonics, Departments of Biology and Chemistry, University of Miami, 1301 Memorial Drive, Coral Gables, Florida 33146-0431, United States

Abstract

A photochemical strategy to encode fluorescence signals *in vivo* with spatial control was designed around the unique properties of a photoactivatable borondipyrromethene (BODIPY). The photoinduced disconnection of two oxazines, flanking a single BODIPY, in two consecutive steps produces a mixture of three emissive molecules with resolved fluorescence inside polymer beads. The relative amounts and emission intensities of the three fluorophores can be regulated precisely in each bead by adjusting the dose of activating photons to mark individual particles with distinct codes of fluorescence signals. The visible wavelengths and mild illumination sufficient to induce these transformations permit the photochemical barcoding of beads also in living nematodes. Different regions of the same animal can be labeled with distinct barcodes to allow the monitoring of their dynamics for long times with no toxic effects. Thus, our photochemical strategy for the generation of fluorescence barcodes can produce multiple and distinguishable labels in the same biological sample to enable the spatiotemporal tracking of, otherwise indistinguishable, targets.

Most experimental studies in chemical research require the manipulation of collections of identical species, ranging from small molecules to large particles, diffusing in fluids and base their conclusions on the average behavior of such a multitude of components. Synthetic protocols rely on the combination of multiple copies of complementary reactants in solution to allow their chemical reaction and the generation of multiple copies of a target product.[1] However, they cannot provide information on the fate of the individual components of the reacting mixture to establish which reactant molecule is converted into which product molecule. The overwhelming challenge in monitoring the evolution of specific individuals in large populations of species extends also to the biological world. The processes responsible

[*]Corresponding Author: fraymo@miami.edu.

[†]**Author Contributions**

These authors contributed equally.

ORCID

Yang Zhang: 0000-0003-1011-3001

Kevin M. Collins: 0000-0001-9930-0924

Françisco M. Raymo: 0000-0002-6163-6606

Notes

The authors declare no competing financial interest.

Supporting Information

The Supporting Information is available free of charge on the ACS Publications website at DOI: 10.1021/jacs.8b00887.

Experimental procedures; chromatograms and photo-kinetic analysis; absorption and emission spectra; photo-chemical and photophysical parameters; fluorescence images (PDF)

Sequential fluorescence images (AVI, AVI)

for embryogenesis demand multiple cells to migrate in the interior of developing embryos and assemble into diverse tissues to generate distinct organs.[2] Tracking the progression of individual cells with spatiotemporal precision to establish where a given cell ultimately localizes in a certain organ is a daunting task. Similar analogies can be extended to behavioral biology, which requires the need to monitor selected individuals in large populations of animals for long times.[3] The development of a general tool to mark chosen members of collections of identical species, ranging from molecules to cells and developed organisms, with recognizable labels that allow their spatiotemporal tracking with minimal perturbation on their behavior would, therefore, be of utmost significance across the biological and chemical sciences. These considerations prompted us to design a photochemical strategy to encode optical barcodes,[4–7] each consisting of multiple fluorescence signals, within selected members of a given population of components with microscaled precision. Our method relies on the photochemical and photophysical properties of photoactivatable fluorophores[8–13] to write optical codes with spatial control and track the marked species in time with the sequential acquisition of fluorescence images. This communication reports the implementation of this mechanism and demonstrates its ability to differentiate and monitor simultaneously multiple species for long times *in vivo*.

Our laboratories recently developed a mechanism for fluorescence activation based on the photochemical behavior of 2*H*,4*H*-[1,3]oxazines[14] and the photophysical properties of borondipyrromethene (BODIPY).[15–19] Our studies ultimately identifed a viable structural design to shift bathochromically the main absorption of a BODIPY with the photoinduced cleavage of an oxazine.[20–24] The resulting spectral shift can be exploited to excite selectively the photochemical product and allow the activation of its fluorescence with ultrahigh contrast levels that would be impossible to achieve with conventional mechanisms based on the photoinduced suppression of quenching pathways.[25–29] These results suggested the design of a compound (**1** in Figure 1) able to undergo two consecutive photochemical reactions. It incorporates a BODIPY and two photocleavable oxazines within the same covalent skeleton and can be synthesized in two steps from known precursors (Figure S1). Upon illumination at an activation wavelength (λA_c) within the spectral region where the 2-nitrobenzyl chromophores absorb, the two oxazines cleave to convert **1** into **2** and then **2** into **3** with the release of two equivalents of **4** (Figure 1). HPLC traces show the gradual decrease of a peak for **1** with the concomitant increase of peaks for **2** and **3**, during the photolytic transformation (Figure S2). The dependence of the relative peak intensities on the irradiation time (Figure S3) indicates the quantum yields (Table S1) for the two consecutive photochemical reactions to be 0.001 and 0.003, respectively.

The absorption and emission spectra (Figures 2a,d and S4) of **1** show bands with maxima at wavelengths of 574 and 587 nm, respectively. The photoinduced disconnection of one of the two 2-nitrobenzyl groups changes the hybridization of the carbon atom in position 2 of the 2*H*,3*H*-indole from sp^3 in **1** to sp^2 in **2**. This structural transformation brings the BODIPY in electronic conjugation with the adjacent indole and shifts bathochromically the absorption and emission bands (Figures 2b,e and S5) to 619 and 628 nm, respectively. The subsequent photoinduced cleavage of the other oxazine converts **2** into **3** and extends the electronic

conjugation of the BODIPY over yet another indole. As a result, the absorption and emission bands (Figures 2c,f and S6) shift further to 663 and 673 nm, respectively.

The pronounced spectral shifts associated with the transformation of **1** into **2** and **3** permit the monitoring of the gradual conversion of these species with the sequential acquisition of absorption and emission spectra (Figure S7), during the photolytic transformation. Similarly, the two consecutive photochemical reactions can be probed with the sequential acquisition of fluorescence images of either PMMA films (Figure S8) or PS beads (Figure S9) doped with these photoswitchable compounds. Selected areas of microscaled dimensions within both samples can be irradiated at a λ_{Ac} of 405 nm to induce the two sequential transformations. The resolved emissions of **1**, **2**, and **3** can be recorded in three separate detection channels of the same fluorescence microscope. This protocol allows the regulation of the relative amounts of the three interconverting species, and hence the emission intensities detected in the three channels, in any illuminated area simply by controlling the irradiation time. For example, PS beads with an average diameter of 3.0 μm can be doped with **1** (5% w/w), deposited on glass and imaged in transmittance mode (Figure 3a). Different regions of the sample can be illuminated individually at λ_{Ac} with identical power, but for four distinct times. Then, fluorescence images of the activated sample can be recorded in three detection channels and overlapped in a single frame (Figure 3b). The emission in one channel (green) can be collected at wavelengths (λ_{Em}) ranging from 575 to 600 nm, upon illumination at an excitation wavelength (λ_{Ex}) of 561 nm, to detect predominantly the fluorescence of **1**. The emission in the other two channels (red and blue) can instead be recorded at λ_{Em} of 645–660 and 750–800 nm, respectively, with a λ_{Ex} of 633 nm in both instances to detect predominantly the fluorescence of **2** and **3**, respectively. A plot (Figure 3c) of the resulting red and blue emission intensities, relative to the green, reveals that nonactivated and activated beads can be distinguished. Each one of these five beads has a unique combination (barcode) of emission values that allows their differentiation. Thus, individual members of a large population of identical beads can be marked photochemically with distinct barcodes to permit the identification of these, otherwise undistinguishable, objects. Furthermore, the ratio-metric quantiflcation of the barcodes eliminates the influence of possible inconsistencies in dopant loading across the beads on the fluorescence signals. Under these conditions, multiple distinguishable barcodes can be imprinted in the same sample simply by adjusting the dose of activating photons (Figures S8 and S9).[30] Additionally, the sequential acquisition of spectra (Figure S10) and fluorescence images (Figure S11) reveals the three fluorophores and the barcodes imprinted in each bead to be stable for prolonged periods of time.

The mild visible illumination sufficient to induce the transformation of **1** into **2** and **3** suggests that it should be possible to write barcodes *in vivo* with no toxic effects. Specifically, the nematode *C. elegans* can be incubated with an aqueous dispersion of PS beads, doped with **1**, to allow the uptake of the fluorescent particles via pharyngeal pumping into the intestine. Sequential fluorescence images (Video S1) reveal bead accumulation in the gut lumen, consistently with a previous study.[31] Treatment of the labeled worms with muscimol, a GABA-A receptor agonist,[32] paralyzes the organism[33] to allow stable illumination and photoconversion of particles within distinct regions of the gut lumen.

Overlaps of fluorescence images, collected in the three detection channels before and after (Figure 4a,b) irradiation exclusively within the posterior intestine, demonstrate that the photochemical transformation is restricted to the illuminated region. Magnifications of the activated area, recorded before (Figure 4c) and after illumination for 5, 10, or 20 min (Figure 4d–f), together with the corresponding barcodes (Figure 4g), confirm the conversion of **1** into **2** and **3**.

The same protocol can be used to write separate barcodes in distinct regions of the same animal and monitor them in time. For example, a worm can be incubated with the doped PS beads and immobilized with muscimol. Illumination of three regions at λ_{Ac} for different times produces distinct amounts of **1**, **2**, and **3**. Comparison of the corresponding images (Figure 5c,e,g) to those (Figures 5d,f and S12) of nonactivated regions confirms the photochemical conversion. Each activated area shows a unique barcode (Figure 5h) that differs from those of the nonactivated areas.

Worms paralyzed with muscimol desensitize and resume normal activity within a few hours. Sequential fluorescence images (Video S2), collected during this time, demonstrate that animals survive bead uptake and irradiation conditions. Furthermore, the imprinted barcodes are stable for prolonged periods of time (Figure S11) and allow tracking of the labeled areas, during muscimol recovery. For example, four images collected consecutively show the translocation of beads from one barcoded region (2 in Figure 6a–d) along the intestinal tract of the animal. Pumping of the pharynx temporarily pushes adjacent beads posteriorly, while the other two barcoded regions (1 and 3 in Figure 6a–d) maintain their original positions. During these dynamic processes, the relative emission intensities of the three channels in each region remain approximately constant, and the barcodes detected before and after pumping are essentially identical (Figure 6e).

In summary, the consecutive disconnection of two photo-cleavable oxazines from the same BODIPY, under the influence of mild visible illumination, generates mixtures of three fluorophores with resolved emissions inside polymer beads. The illumination conditions can be adjusted to regulate precisely the relative amounts of the three emissive species to imprint barcodes, each consisting of three fluorescence signals, within individual beads. Furthermore, selected members of large populations of beads can be marked with unique and detectable codes to allow their individual tracking in time. The visible wavelengths and moderate intensities, sufficient to induce these transformations, permit the photochemical imprinting of barcodes also in living worms. Different regions of the same animal can be marked with distinct barcodes and their dynamics tracked for long times. Thus, our mechanism for photochemical barcoding can evolve into a general strategy for the imprinting of multiple, but distinguishable, labels *in vivo* with unprecedented spatial and temporal control.

Supplementary Material

Refer to Web version on PubMed Central for supplementary material.

Acknowledgments

The National Institutes of Health (NS086932) and National Science Foundation (CHE-1505885) are acknowledged for financial support.

References

1Corey EJ, , Cheng X-M. The Logic of Chemical Synthesis Wiley; New York: 1995

2Wolpert L, , Tickle C. Principles of Development Oxford University Press; Oxford: 2010

3Dugatkin LA. Principles of Animal Behavior Norton & Company; 2014

4Jun BH, Kang H, Lee YS, Jeong DH. Molecules. 2012; 17:2474–2490. [PubMed: 22382526]

5Gorris HH, Wolfbeis OS. Angew Chem, Int Ed. 2013; 52:3584–3600.

6Leng Y, Sun K, Chen X, Li W. Chem Soc Rev. 2015; 44:5552–5595. [PubMed: 26021602]

7Shikha S, Salafi T, Cheng J, Zhang Y. Chem Soc Rev. 2017; 46:7054–7093. [PubMed: 29022018]

8Wysocki LM, Lavis LD. Curr Opin Chem Biol. 2011; 15:752–759. [PubMed: 22078994]

9Puliti D, Warther D, Orange C, Specht A, Goeldner M. Bioorg Med Chem. 2011; 19:1023–1029. [PubMed: 20675143]

10Li WH, Zheng G. Photochem Photobiol Sci. 2012; 11:460–471. [PubMed: 22252510]

11Raymo FM. J Phys Chem Lett. 2012; 3:2379–2385. [PubMed: 26292118]

12Klán P, Šolomek T, Bochet CG, Blanc A, Givens R, Rubina M, Popik V, Kostikov A, Wirz J. Chem Rev. 2013; 113:119–191. [PubMed: 23256727]

13Raymo FM. Phys Chem Chem Phys. 2013; 15:14840–14850. [PubMed: 23780303]

14Deniz E, Tomasulo M, Cusido J, Sortino S, Raymo FM. Langmuir. 2011; 27:11773–11783. [PubMed: 21591642]

15Benstead M, Mehl GH, Boyle RW. Tetrahedron. 2011; 67:3573–3601.

16Boens N, Leen V, Dehaen W. Chem Soc Rev. 2012; 41:1130–1172. [PubMed: 21796324]

17Kamkaew A, Lim SH, Lee HB, Kiew LV, Chung LY, Burgess K. Chem Soc Rev. 2013; 42:77–88. [PubMed: 23014776]

18Lu H, Mack J, Yang Y, Shen Z. Chem Soc Rev. 2014; 43:4778–4823. [PubMed: 24733589]

19Ni Y, Wu J. Org Biomol Chem. 2014; 12:3774–3791. [PubMed: 24781214]

20Zhang Y, Swaminathan S, Tang S, Garcia-Amorós J, Boulina M, Captain B, Baker JD, Raymo FM. J Am Chem Soc. 2015; 137:4709–4719. [PubMed: 25794143]

21Garcia-Amoros J, Swaminathan S, Zhang Y, Nonell S, Raymo FM. Phys Chem Chem Phys. 2015; 17:11140–11143. [PubMed: 25855103]

22Zhang Y, Tang S, Sansalone L, Baker JD, Raymo FM. Chem - Eur J. 2016; 22:15027–15034. [PubMed: 27571689]

23Thapaliya ER, Zhang Y, Raymo FM. J Mater Chem C. 2017; 5:1179–1183.

24Liu X, Zhang Y, Baker JD, Raymo FM. J Mater Chem C. 2017; 5:12714–12719.

25Kobayashi T, Komatsu T, Kamiya M, Campos C, González-Gaitán M, Terai T, Hanaoka K, Nagano T, Urano Y. J Am Chem Soc. 2012; 134:11153–11160. [PubMed: 22694089]

26Shaban Ragab S, Swaminathan S, Deniz E, Captain B, Raymo FM. Org Lett. 2013; 15:3154–3157. [PubMed: 23738708]

27Shaban Ragab S, Swaminathan S, Baker JD, Raymo FM. Phys Chem Chem Phys. 2013; 15:14851–14855. [PubMed: 23694991]

28Amamoto T, Hirata T, Takahashi H, Kamiya M, Urano Y, Santa T, Kato M. J Mater Chem B. 2015; 3:7427–7433.

29Goswami PP, Syed A, Beck CL, Albright TR, Mahoney KM, Unash R, Smith EA, Winter AH. J Am Chem Soc. 2015; 137:3783–3786. [PubMed: 25751156]

30The blue bar in most barcodes (Figures 3–6, S8, and S9) appears lower than the red one because of the choice in detection wavelengths. Specifically, the fluorescence in the blue channel was collected from 750 to 800 nm only to ensure a minimal contribution of **2** (Figure 2e) to the

detected intensity. This spectral window covers only the tail of the emission band of **3** (Figure 2f). As a result, only a fraction of its fluorescence is considered in the quantification of the barcodes.

31Frølund B, Ebert B, Kristiansen U, Liljefors T, Krogsgaard-Larsen P. Curr Top Med Chem. 2002; 2:817–832. [PubMed: 12171573]

32Fang-Yen C, Avery L, Samuel AD. Proc Natl Acad Sci U S A. 2009; 106:20093–20096. [PubMed: 19903886]

33Collins KM, Koelle MR. J Neurosci. 2013; 33:761–775. [PubMed: 23303953]

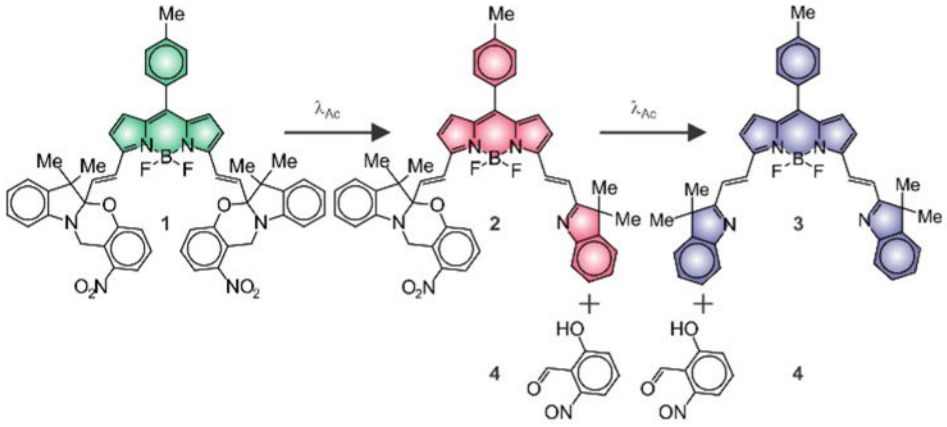

Figure 1.
Photoinduced transformation of **1** into **2**, **3**, and **4**.

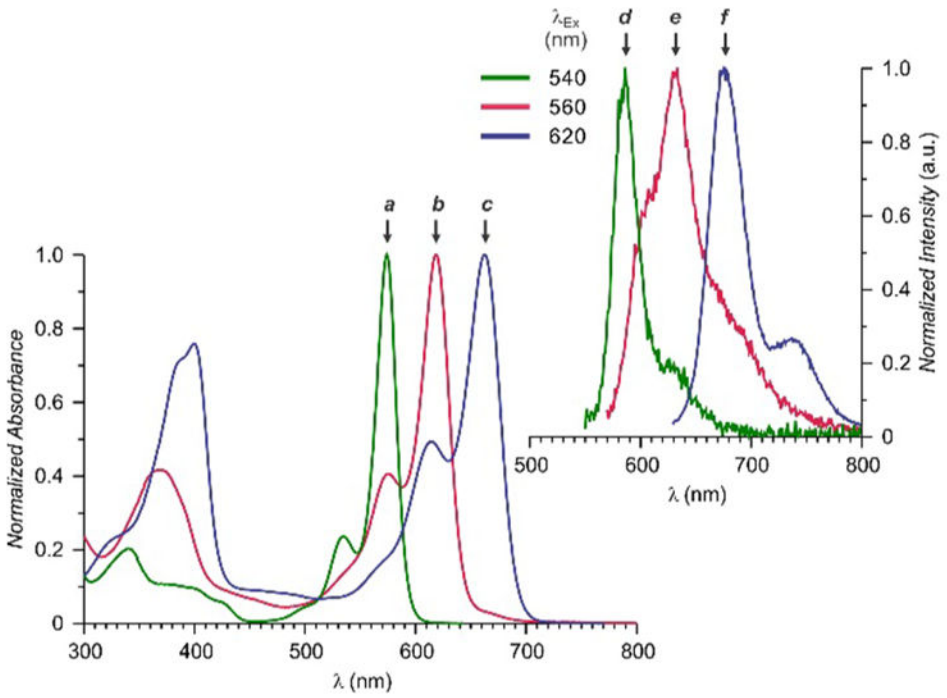

Figure 2.

Normalized absorption and emission spectra of **1** (a,d) **2** (b,e), and **3** (c,f) in MeCN at 25 °C.

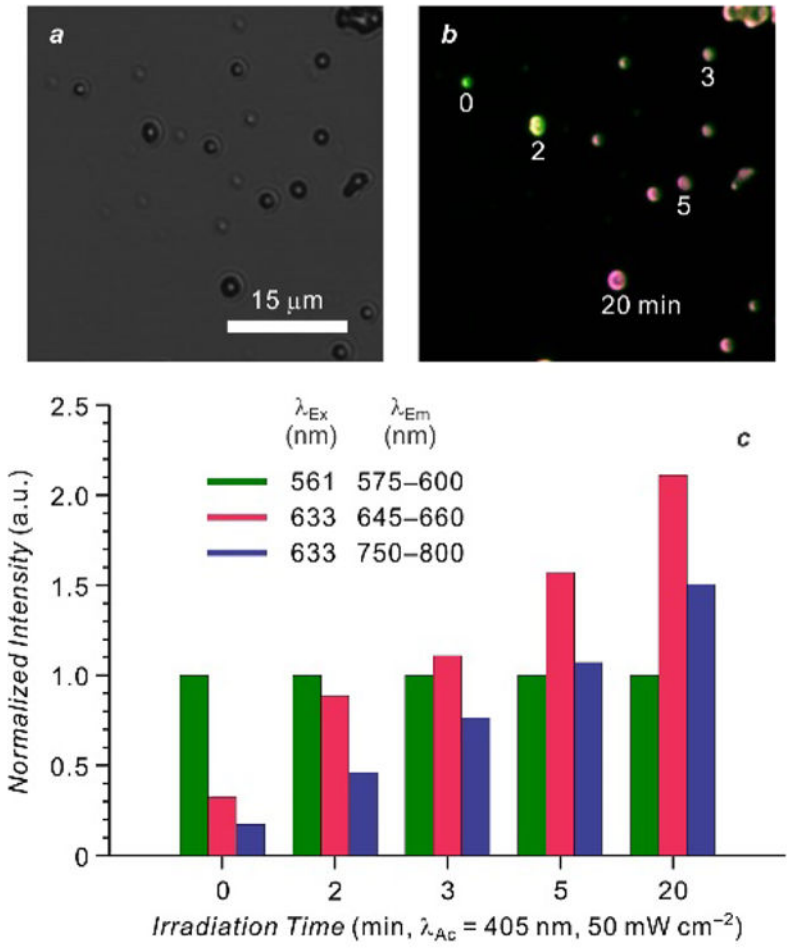

Figure 3.

Brightfield image (a), overlap of three fluorescence channels (b), and relative emission intensities (c) of PS beads, doped with **1** (5% w/w), recorded after irradiation of individual beads for different times.

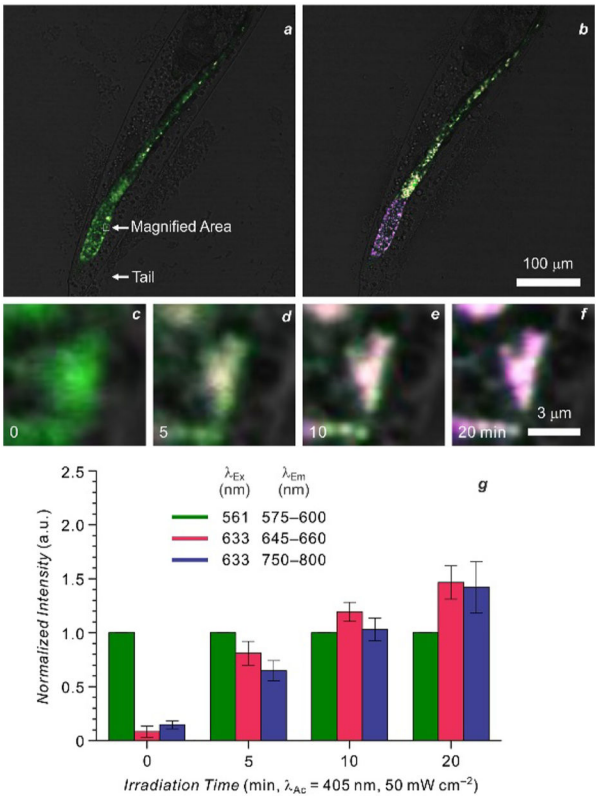

Figure 4.

Overlaps of brightfield images and three fluorescence channels of *C. elegans* labeled with PS beads, doped with **1** (5% w/w), recorded before (a) and after (b) irradiation of the tail for 20 min; magnifications acquired before (c) and after (d–f) illumination for increasing times and relative emission intensities (*g*).

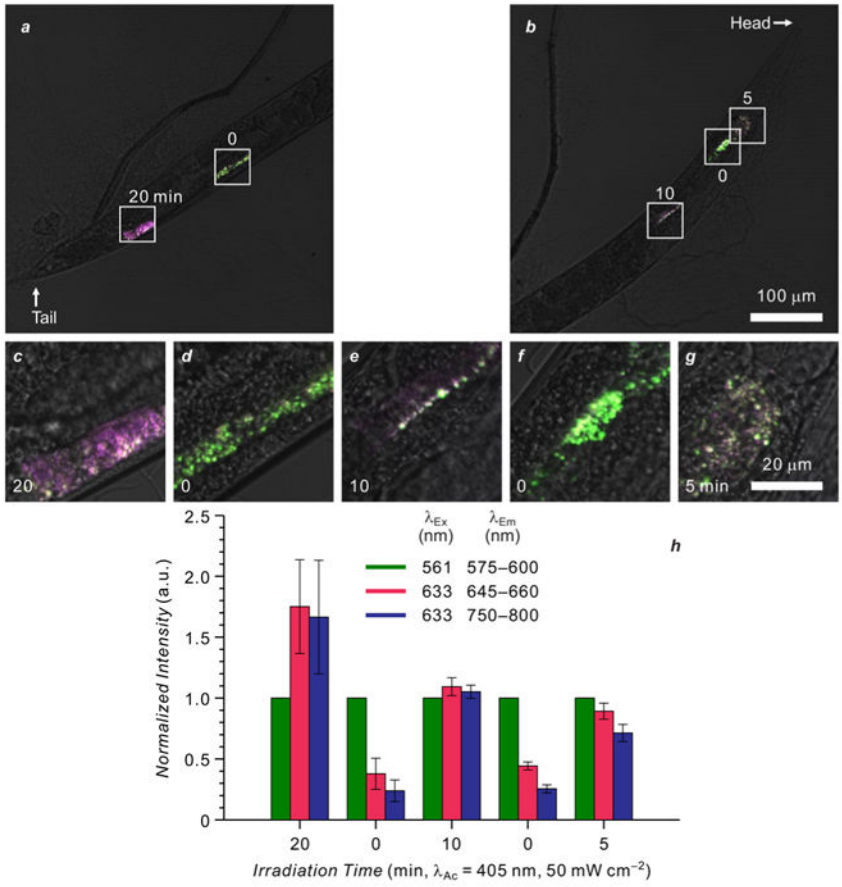

Figure 5.

Overlaps (a,b) of brightfield images and three fluorescence channels of *C. elegans* labeled with PS beads, doped with **1** (5% w/w), recorded after irradiation of distinct regions for different times; magnifications of nonirradiated (d,f) and irradiated (c,e,g) areas and relative emission intensities (h).

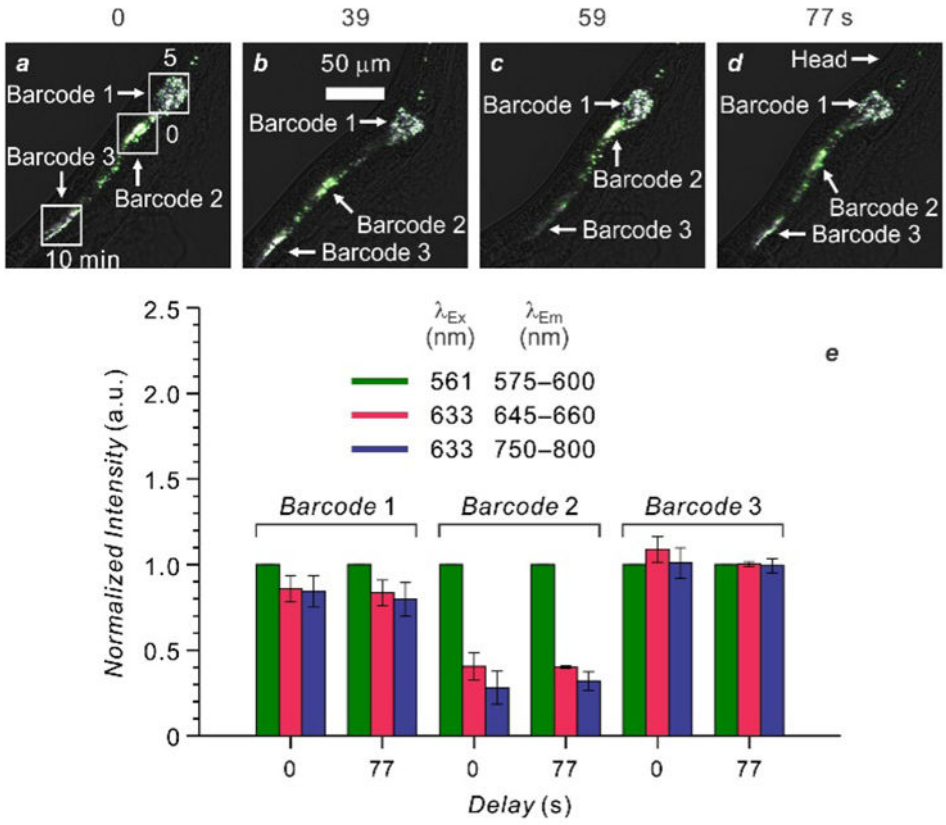

Figure 6.

Overlaps of brightfield images and three fluorescence channels (a–d) of *C. elegans* labeled with PS beads, doped with **1** (5% w/w), recorded sequentially over 77 s after irradiation of distinct regions for different times and storage for 50 min, and relative emission intensities (e) in the initial (a) and final (d) frames.